Collinear Invariant Shapes for Three-Spacecraft Coulomb Formations

Erik Hogan and Hanspeter Schaub

Simulated Reprint from

Acta Astronautica

Vol. 12, March–April 2012, pp. 78–89

COLLINEAR INVARIANT SHAPES FOR THREE-SPACECRAFT COULOMB FORMATIONS

Erik Hogan[a,1,*], Hanspeter Schaub[a,2]

[a] *University of Colorado, Boulder, CO 80309-0431*

Abstract

This paper investigates invariant shape conditions for a three-craft collinear formation in deep space controlled solely by electrostatic Coulomb forces. Previous research shows that invariant shape solutions can exist under certain circumstances for a charged three-craft collinear configuration. This paper investigates the structure of the cluster shape solution space. The problem is examined from a mission design perspective, determining whether or not real charges can always be found that will yield a desired invariant collinear shape configuration. The paper proves that for any three-craft collinear invariant shape formations there always exists an infinite set of real open-loop charges that yield a shape equilibrium. Further, the null-space of the feasible charge solutions is analyzed, and a method for determining a charge-optimal solution is presented. The results are demonstrated through use of numerical simulations.

Keywords: formation flying, Coulomb formations, invariant shape solutions

1. Introduction

Close formation flying of satellites, with separation distances ranging on the order of tens of meters, presents many exciting space mission possibilities. By maintaining several different satellites within tens of meters of one another, a significant amount of scientific instrumentation can be concentrated in a small area of space. This type of formation has several advantages over a single large craft. Not all of the satellites need to be launched at the same time. Individual craft can take advantage of available space on already scheduled launch vehicles. This allows for the assembly of a formation over a period of time, rather than all at once. By designing a formation that does not require a physical structure to hold the components together, complicated space-based assemblies are avoided. Satellites can theoretically be launched into their position in the formation and start integration and operation immediately. Because the considered separation distances between each craft are as large as tens of meters, scientific instruments are spaced farther apart, which is challenging on a single craft. Finally, the significant advantage of a free-flying virtual structure is that the formation shape and size can be changed to accommodate new mission requirements by applying a new control strategy. This type of formation is of interest to interferometry applications such as the proposed Terrestrial Planet Finder.[1, 2]

A particular challenge present in close formation flying research is the actuation method used to maintain the formation. Traditional propellant thrusters eject significant amounts of particles which can interfere with sensitive instrumentation onboard another nearby craft.[3] This concern is called the plume impingement issue, and is very challenging when the vehicles are to operate only dozens of meters apart. An alternative to using traditional thrusters is electrostatic, or Coulomb, force actuation.[4, 5, 6] By controlling the charges on individual spacecraft, electrostatic forces are generated to maintain the shape of a particular formation.[7] This type of control is nearly propellantless, and operates at a very high specific impulse (up to 10^{13} seconds).[3, 8] Further advantages to using electrostatic force

*Corresponding author

Email addresses: erik.hogan@colorado.edu (Erik Hogan), hanspeter.schaub@colorado.edu (Hanspeter Schaub)

URL: http://hanspeterschaub.info (Hanspeter Schaub)

[1] Graduate Student, Department of Aerospace Engineering Sciences, University of Colorado

[2] Associate Professor, H. Joseph Smead Fellow, Department of Aerospace Engineering Sciences, University of Colorado

actuation include a very minimal power requirement on the order of Watts or less, and very rapid charge times on the order of milliseconds.[8] The charge levels proposed to implement this type of control are on the order of micro-Coulombs (μC). Such charge concentrations naturally occur on spacecraft in geosynchronous orbit (GEO) regimes during shaded orbit segments, and result in forces on the milli- or micro-Newton levels for craft separated by tens of meters.[6, 9] In order to implement Coulomb force control, however, natural charging would not be acceptable due to the fact that very specific charge levels are needed for the desired formation shape actuation. Simply allowing the craft to charge naturally would not result in the necessary charge levels to achieve a desired dynamic relative motion response. Instead, the craft would need to be able to perform active charge control. Fortunately, active charge control has been demonstrated in orbit on both the SCATHA and ATS missions in the 1970's,[10, 11, 12, 13] as well as in the current European CLUSTER mission.[14, 15] The drawback to using Coulomb force actuation is the high sensitivity to the plasma environment around the spacecraft. Electrostatic force control can only be used in a plasma environment with a large Debye length, λ_D, (on the order of tens of meters or more) due to the shielding effect caused by the plasma.[3] As such, Coulomb formation flying is best suited to higher Earth orbit regimes or deep space (interstellar) applications.

Of particular interest in Coulomb formation flying are constant charge invariant shape configurations in which several craft maintain separation distances on the order of tens of meters. Here the spacecraft appear stationary or frozen with respect to the circularly rotating formation center of mass frame.[5] Such formations are investigated by Berryman and Schaub in Reference [16] where analytic charge solutions are determined for 2- and 3-craft formations in geosynchronous orbit, while Reference [17] investigates necessary conditions for such charged virtual space structure solutions to exist. In Reference [16] the authors examine issues related to such charged relative equilibria requiring imaginary charges for particular configurations. Another type of invariant shape Coulomb formation is investigated by Hussein et al. in Reference [18], with a focus on deep space applications. Here three-craft formations are examined which orbit about their collective center of mass in the absence of gravity. In contrast to the earlier Coulomb virtual structures that are static relative to the orbiting Hill frame, here the charged spacecraft system is spinning. It is this type of invariant shape formation which serves as the inspiration for the current work. A rotating three-craft collinear equilibrium case for deep space applications is the focus of this paper. Hussein et al. describe the necessary conditions for invariant shape formations of three-craft in a collinear formation, and extend this analysis to determining geometrical configurations that yield invariant shapes given a particular set of charges.[18] Determining a solution for the reverse case has not been performed as of yet; for example, given a specific geometrical configuration and formation orbital parameters, determine a solution for the charges on the individual spacecraft. Previous work primarily focuses on defining the requirements for collinear invariant shape formation. No analysis has been done from a mission design standpoint. With this consideration in mind, an extension of previous work is performed to enable the design of a particular geometric configuration for a three-craft invariant shape solution. Of interest is whether or not any desired configuration shape is possible with real and constant charges, or whether or not the nature of using electrostatic actuation will limit the set of realizable invariant shapes.

The paper is structured as follows. First, a brief introduction to the concept of Coulomb formation flying, and invariant shape solutions in particular is provided, followed by a brief overview of some fundamental concepts of spinning charged spacecraft equilibria. Next, the simplified equal mass case is presented to aid with clarity in understanding the theory behind the solution method. The simplified mathematics corresponding to this case allow for a more succinct introduction to the problem. After covering the simplified case, the more general problem of a non-equal mass formation is covered in detail, including how to determine an optimal solution that minimizes the charge usage. It is at this point that the concept of orbit design for an invariant shape solution is covered. Once the theory behind the solution method is established, it is applied to example cases and numerical simulations are used to demonstrate and validate the results.

2. Background

2.1. Coulomb Formation Flying

Before proceeding through the development, it is pertinent to discuss the basic theory behind Coulomb formation flying and briefly introduce the concept of an invariant shape formation. The scope of this paper is limited to a Coulomb formation of three-craft, as depicted in Fig. 1. As in the prior work in Reference [18], each craft is treated

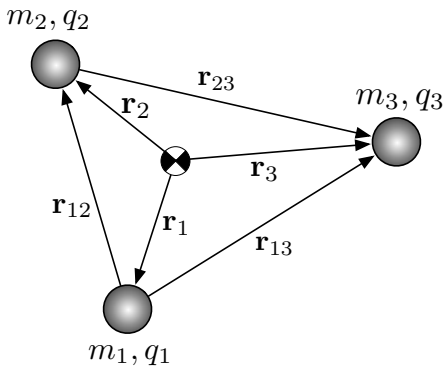

Figure 1: The three-craft Coulomb formation.

as a particle with mass m_i and charge q_i. The vectors $\mathbf{r}_1$, $\mathbf{r}_2$, and $\mathbf{r}_3$ are the position vectors from the formation center of mass to each of the three craft. The relative position vectors $\mathbf{r}_{ij}$ are defined as $\mathbf{r}_{ij} = \mathbf{r}_j - \mathbf{r}_i$. In the absence of any external forces, such as gravity, the dynamics of any single craft in the formation are influenced only by inter-craft electrostatic forces. Due to the fact that Coulomb forces are internal to the formation[3] and no formation-external forces are considered, the center of mass must satisfy the constraint condition

$$M\ddot{\mathbf{r}}_c = \mathbf{0}, \tag{1}$$

where $M = m_1 + m_2 + m_3$. Thus, the center of mass of the formation is inertial. To arrive at the equation of motion for a single craft in the formation, the electric potential of a particle in a plasma environment with a finite Debye length, λ_D, is examined first.[19] For a particle with charge q, the potential at a distance r is given as

$$\phi(r) = k_c \frac{q}{r} \mathrm{e}^{-r/\lambda_D}, \tag{2}$$

where $k_c = 8.99 \times 10^9$ Nm^2/C^2 is the Coulomb constant. This simple analytical solution for the potential about a point charge or sphere assumes that the potential of the object is relatively small in comparison to the local plasma temperature.[20] For example, at geosynchronous orbit altitudes where the spacecraft fly the Earth's plasma sheath, this potential threshold is about 1-10 kV. If the full Poisson-Vlaslov partial differential electrostatic field equations are solved instead of using a truncated version that yields the simple analytical result in Eq. (2), then large potentials can reduce the plasma charge shielding effect. This Coulomb force behavior is discussed in Reference [21] where the use of an electrostatic force to move an asteroid in deep space is discussed. For example, effective Debye lengths that are multiple times the conventional Debye lengths have been computed.

The electric field created by the potential distribution $\phi(\mathbf{r})$ is defined as

$$\mathbf{E} = \nabla_{\mathbf{r}} \phi. \tag{3}$$

The full equations of motion for a craft in the Coulomb formation is then determined by the dynamics of a charged particle in an electric field. For craft i in the formation, the equations of motion are determined as

$$m_i \ddot{\mathbf{r}}_i = q_i \mathbf{E} = \sum_{j=1, j\neq i}^{3} k_c \frac{q_i q_j}{r_{ij}^2} \mathrm{e}^{-r_{ij}/\lambda_D} \left(1 + \frac{r_{ij}}{\lambda_D}\right) \hat{\mathbf{n}}_{ji} \tag{4}$$

where $\hat{\mathbf{n}}_{ji}$ is the unit vector from craft j to craft i. Much of the development in this paper applies to the case where the local separation distances are much less than the effective Debye length of the surrounding plasma environment ($r_{ij} \ll \lambda_D$). While it is true that Debye lengths in the interplanetary medium at 1 AU from the sun can be 30-50 meters,[5] on the order of the craft separation distances, objects charged to high potentials (>1 kV) will experience effective Debye lengths many times larger.[21] Considering that such potential levels are proposed for Coulomb force

actuation[3], it is a reasonable approximation to assume minimal Debye shielding effects for the current study. The electrostatic force $\mathbf{F}_c = q_i\mathbf{E}$ in Eq. (4) must be considered a conservative lower bound on the achievable Coulomb actuation, while treating $\lambda_D \to \infty$ provides the upper bound used in this paper. Using the conservative analytical Debye shielding expression in Eq. (4) with the exponentially decaying terms makes analytical insight into the charged dynamical motion more complex, and limits the potential solution space of invariant shape motion.[18] The primary results presented in this paper are obtained using the large Debye length assumption, which is weakly valid for craft charged to 10's of kilo-Volts. For the sake of completeness, however, the full finite-Debye length case is considered following the results from the large Debye length case.

2.2. Invariant Shape Solutions

Hussein et al. describe the first solutions for the spinning invariant shape Coulomb formation[18]. In their analysis, a three-craft formation is considered under the assumption that only inter-craft Coulomb forces are present. Indeed, the development of the necessary conditions to maintain such a formation is dependent on this assumption; invariant shape, center of mass orbiting formations would not be possible in the presence of gravity. This limits their potential immediate applications to deep-space (interstellar) missions where celestial gravitational effects are minimal. In the current work, this assumption is maintained.

An invariant shape is classified as a constant charge configuration that maintains the initial shape of the formation for all time. There is no requirement that the exact dimensions of the shape are maintained for all time, only that the entire shape scales proportionately relative to the initial dimensions. That is, at any time t the formation must satisfy

$$\frac{r_{12}(t)}{r_{12}(0)} = \frac{r_{13}(t)}{r_{13}(0)} = \frac{r_{23}(t)}{r_{23}(0)}. \tag{5}$$

Thus, the separation distances may scale up or down, as long as the side length ratios are maintained. Naturally, it follows that the angular rotation vector of each craft, $\boldsymbol{\omega}_i = \mathbf{r}_i \times \dot{\mathbf{r}}_i$, must be equal at any point in time, so that

$$\boldsymbol{\omega}_1(t) = \boldsymbol{\omega}_2(t) = \boldsymbol{\omega}_3(t). \tag{6}$$

Note that this development of the invariant shape spinning formation of charge vehicles mimics the development of Lagrange's classical approach to the search for invariant shape solutions of the three gravitational bodies.[22, 23]

Recall that the only forces acting on the formation are the inter-craft Coulomb forces that are internal to the formation. As a result, the angular momentum of the formation is constant. It can be shown that as a direct consequence the momenta of each individual craft is constant.[18] Performing a time derivative of the individual craft momenta yields

$$\dot{\mathbf{H}}_i = \mathbf{r}_i \times (m_i\ddot{\mathbf{r}}_i) = \mathbf{r}_i \times \mathbf{F}_i = 0. \tag{7}$$

This result, used by Hussein et al., demonstrates that a necessary condition to maintain an invariant shape formation is that the resulting force vector acting on any craft, $\mathbf{F}_i$, be aligned with the formation center of mass. In their work, the authors identify two different configurations that yield invariant shape solutions for the formation: collinear arrangements and equilateral triangles.

For an equilateral triangle configuration to maintain an invariant shape, all craft must have the same charge polarity.[18] Consequently, all the craft repel each other and the formation shape grows unbounded. Thus, such a configuration is not a practical option for designing a close formation of spacecraft that need to maintain separation distances on the order of tens of meters for a long period of time. A collinear arrangement of craft, however, allows for the craft to remain in close proximity through the use of closed orbits about the formation center of mass. Such a configuration is depicted in Fig. 2. The geometry of a collinear invariant shape is defined by the separation distances r_{12} and r_{23}, which need not be constant. All that is required to satisfy Eq. (5) is that the ratio of the side lengths be constant for all time. This ratio, denoted as χ, is defined as

$$\chi = \frac{r_{23}}{r_{12}} > 0. \tag{8}$$

Because the separation distances are always strictly positive quantities, the value of χ is always greater than zero. The individual separation distances may change with time, so long as they maintain the original value of χ. There are

several potential trajectories for the collinear invariant shape; depending on the configuration, the craft will take on one of the Keplerian orbit types.[18] If the separation distances are to remain fixed, circular trajectories will result. For the case where separation distances grow and shrink in an oscillatory manner, the craft will take on elliptic trajectories. The craft may also grow infinitely far apart on parabolic or hyperbolic trajectories.

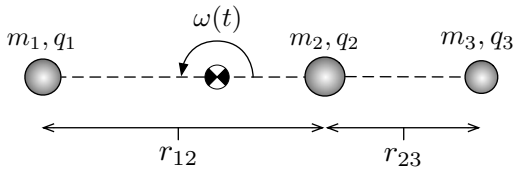

Figure 2: Collinear invariant shape formation of three craft.

The necessary charges required to maintain an invariant shape formation are a function of the craft masses, separation distances, and χ value. For an invariant shape formation to exist, the configuration parameters must satisfy[18]

$$\begin{aligned} 0 =& c_1c_2\left[m_1+\chi(m_1+m_2)\right]\chi^2(1+\chi)^2(1+\frac{r_{21}}{\lambda_D})+c_1c_3(\chi m_3-m_1)\chi^2 e^{-\frac{r_{21}\chi}{\lambda_D}}(1+\frac{r_{21}(1+\chi)}{\lambda_D}) \\ &- c_2c_3(m_2+m_3+\chi m_3)(1+\chi)^2 e^{\frac{r_{21}(1-\chi)}{\lambda_D}}(1+\frac{r_{21}\chi}{\lambda_D}), \end{aligned} \tag{9}$$

where $c_i = q_i/m_i$ is the specific charge of each craft. Note that the form of Eq. (9) is modified slightly from that of Reference [18], where the simple, and overly conservative, plasma-shielded electrostatic force expression $\mathbf{F} = k_c\frac{q_1q_2}{r^2}e^{-r/\lambda_D}$ is used. Equation (9) provides a means to determine a necessary χ value if given a set of charges, or vice-versa. Previous work investigates the determination of an appropriate χ if given a set of charges. From a mission design standpoint, this is not ideal. Rather, it would be more useful to be able to design some desired formation geometry and associated spin rate, and then determine a set of charges that would enable such a configuration. This mission design perspective is the focus of the current paper.

3. Problem Statement

3.1. Equal Mass Case

Reference [18] demonstrates a method for determining a solution to the invariant shape case with a given charge configuration. This work extends the solution for the collinear invariant shape Coulomb formation by developing a method to determine charge configurations which will yield a desired orbital configuration about the center of mass. Let us first examine the solution space for a configuration where all craft have equal mass, that is, $m_1 = m_2 = m_3$. Furthermore, assume the craft are operating in an environment with large Debye lengths. With these assumptions, Eq (9) is simplified to

$$-2q_2q_3 - 5q_2q_3\chi + (q_1q_2 - q_1q_3 - 4q_2q_3)\chi^2 + (4q_1q_2 + q_1q_3 - q_2q_3)\chi^3 + 5q_1q_2\chi^4 + 2q_1q_2\chi^5 = 0 \tag{10}$$

Recall that the goal of this work is to determine a charge solution for a given configuration. Consider a particular mission where a certain χ is needed to obtain a desired shape. In order to satisfy the requirements for a three-craft equilibrium formation, charge values must be determined which satisfy Eq. (10) for the desired χ value. In its current form, Eq. (10) is nonlinear with respect to the individual charges. However, by replacing the actual charges with the charge products

$$Q_{ij} = q_iq_j$$

the system becomes linear. Once a solution for the charge products is obtained, the individual vehicle charges can be determined from[16]

$$q_1 = \sqrt{\frac{Q_{12}Q_{13}}{Q_{23}}} \tag{11a}$$

$$q_2 = \frac{Q_{12}}{q_1} \tag{11b}$$

$$q_3 = \frac{Q_{13}}{q_1}. \tag{11c}$$

This formulation, however, leads to an important constraint. In order to determine real charge values for each craft, it required that $Q_{12}Q_{13}Q_{23} > 0$.[16] Using the charge product (Q_{ij}) to charge (q_i) mapping described in Eq. (11), the quintic Eq. (10) is rewritten in terms of charge products as

$$Q_{12}\left(2\chi^5 + 5\chi^4 + 4\chi^3 + \chi^2\right) + Q_{13}\left(\chi^3 - \chi^2\right) + Q_{23}\left(-\chi^3 - 4\chi^2 - 5\chi - 2\right) = 0. \tag{12}$$

This is an underdetermined system with three unknowns and only one constraint. There are an infinite number of solutions to to determine necessary charge products Q_{ij}, which are defined by a two-dimensional null space. Rewriting Eq. (12) in matrix form, we obtain

$$[X]\mathbf{Q} = \begin{bmatrix} 2\chi^5+5\chi^4+4\chi^3+\chi^2 & \chi^3-\chi^2 & -\chi^3-4\chi^2-5\chi-2 \end{bmatrix} \begin{bmatrix} Q_{12} \\ Q_{13} \\ Q_{23} \end{bmatrix} = 0 \tag{13}$$

The realm of all allowable charge solutions, then, is described by the $2x3$ null space $[N]$ matrix of the $3x1$ mapping $[X]$,

$$[N] = \begin{bmatrix} \frac{2+\chi}{\chi^2(1+2\chi)} & 0 & 1 \\ \frac{1-\chi}{(1+2\chi)(1+\chi)^2} & 1 & 0 \end{bmatrix}. \tag{14}$$

Now, each charge product may be written in terms of a nominal solution, $\hat{Q}_{ij}$, which satisfies Eq. (12), and the null space such that

$$Q_{12} = \hat{Q}_{12} + \gamma_1 \frac{2+\chi}{\chi^2(1+2\chi)} + \gamma_2 \frac{1-\chi}{(1+2\chi)(1+\chi)^2} \tag{15a}$$

$$Q_{13} = \hat{Q}_{13} + \gamma_2 \tag{15b}$$

$$Q_{23} = \hat{Q}_{23} + \gamma_1, \tag{15c}$$

where γ_1 and γ_2 are real scaling parameters of any arbitrary value. By inspection, it is evident that $\mathbf{Q} = \mathbf{0}$ is a nominal solution which satisfies Eq. (12). This nominal solution can be used to determine which values of γ_1 and γ_2 are acceptable given the inequality constraint $Q_{12}Q_{13}Q_{23} > 0$. Using Eqs. (15) and the nominal solution $\mathbf{Q} = \mathbf{0}$, this inequality can be expressed as

$$\gamma_1\gamma_2\left(\gamma_1 \frac{2+\chi}{\chi^2(1+2\chi)} + \gamma_2 \frac{1-\chi}{(1+2\chi)(1+\chi)^2}\right) > 0. \tag{16}$$

In order to determine real charge solutions for each of the craft, it is necessary to find values of γ_1 and γ_2 that satisfy the inequality in Eq. (16). Notice that in the null space, there is only one possibility of a sign change among the six elements. This occurs in $[N]_{(2,1)}$, and is dependent on the value of χ. Recalling that the only constraint on χ is that it be greater than zero, three different cases arise which must be analyzed. To analyze permissible regions of γ_1 and γ_2 values, a two-dimensional cartesian coordinate system, as depicted in Fig. 3, is used. The horizontal axis corresponds to the γ_1 parameter, while the vertical axis corresponds to the γ_2 parameter.

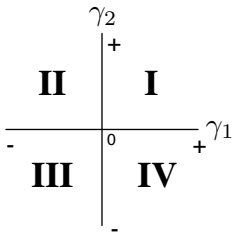

Figure 3: $\gamma_1 - \gamma_2$ axes used in discussion of permissible regions.

Case 1: $0 < \chi < 1$
When χ is between 0 and 1, the permissible regions of γ_1 and γ_2 are defined by the line

$$\gamma_2 = \frac{(1+\chi)^2(2+\chi)}{(\chi-1)\chi^2}\gamma_1. \tag{17}$$

Due to the value of χ the $\chi - 1$ term will be negative, leading to a line with a negative slope. In this case, any values in quadrant I are acceptable. In quadrant II, any values below the line in Eq. (17) are permissible. Nothing in quadrant III is permissible, and in quadrant IV, values below the line in Eq. (17) are permissible. These regions are illustrated in Fig. 4(a). The regions of the graph that are white are permissible, while the hatched regions are non-permissible.
Case 2: $\chi = 1$
When the value of χ is exactly 1, the inequality in Eq. (16) reduces to

$$\gamma_2 > 0.$$

As a result, all values above the γ_1 axis, not including the axis itself, are permissible. This is illustrated in Fig. 4(b).
Case 3: $\chi > 1$
When $\chi > 1$, the permissible regions of γ_1 and γ_2 are again defined by the line in Eq. (17). In this case, however, the $\chi - 1$ term will be positive, giving the line a positive slope. In quadrant I, values below this line are acceptable. All of quadrant II is a permissible region, while in quadrant III any values below the line in Eq. (17) will satisfy the constraint inequality. No values from quadrant IV are acceptable. These regions are illustrated in Fig. 4(c).

Noting that these three cases describe every possible value for χ, it becomes apparent that a real charge solution can be determined for any desired χ. In fact, there are an infinite number of real solutions. What this analysis does not reveal, however, are the resulting orbits that the three craft must experience to maintain the invariant shape for any given charge solution. Indeed, it is possible that the craft could experience circular, elliptical, or hyperbolic orbits relative to the formation center of mass. While this analysis cannot be used directly to design any specific orbital configuration, it does imply that there are no restrictions on the value of χ for the assumptions made (aside from $\chi > 0$). Knowing this, the design of a particular invariant shape solution can now be analyzed.

3.2. General Mass Case

Returning to the general case where the craft may have different masses (with large Debye lengths maintained), the design of a particular orbital configuration will now be considered. Rather than simply specifying a χ value, desired orbital parameters will also be factored into the solution for the necessary craft charges. Using the same linear form for the charge products as before, Eq. (9) can be expressed as

$$Q_{12}\left(\frac{m_1\chi^2 + (3m_1+m_2)\chi^3 + (3m_1+2m_2)\chi^4 + (m_1+m_2)\chi^5}{m_1m_2}\right)$$
$$+ Q_{13}\left(\frac{-m_1\chi^2 + m_3\chi^3}{m_1m_3}\right) + Q_{23}\left(\frac{-(m_2+m_3) - (2m_2+3m_3)\chi - (m_2+3m_3)\chi^2 - m_3\chi^3}{m_2m_3}\right) = 0, \tag{18}$$

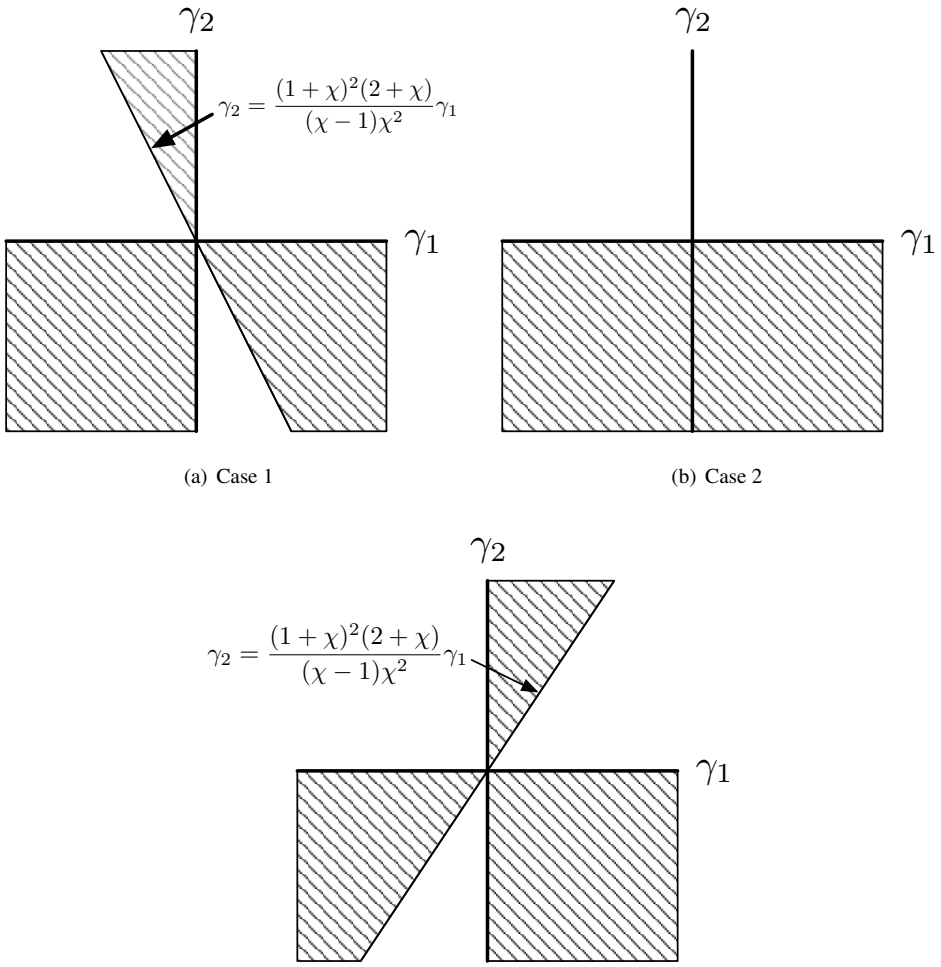

(a) Case 1

(b) Case 2

(c) Case 3

Figure 4: Permissible regions for each of the three cases. Values from white areas will satisfy Eq. (16), while values from hatched areas will not.

providing one constraint equation. To allow further control of craft orbit parameters an alternate form for the craft dynamics, developed by Hussein et al.,[18] is introduced. When the craft are in a collinear invariant shape formation, the motion of each craft is described by

$$\ddot{\mathbf{r}}_i = -\frac{\mu_i}{r_i^3}\mathbf{r}_i, \tag{19}$$

where $\mathbf{r}_i$ is the vector from the center of mass of the formation to craft i and μ_i is a constant, sometimes called the effective gravitational parameter, which is a function of the craft charges, the masses, and χ. It is important to note that the value of μ_i is different for each craft in the formation. In order to maintain an invariant shape, each craft in the formation must have the same mean motion, denoted as n. Furthermore, if a semi-major axis for the orbit of one craft is selected, along with a χ value, the shape of the entire system is defined. When choosing a craft to use in the semi-major axis constraint, it is important to choose either craft 1 or 3 to avoid possible singularity issues. The reason for this is explained further momentarily. For the development here, craft 1 will be used to formulate the second constraint and allow for the design of the resulting craft orbits. Recall that the expression for mean motion of

an orbiting body is

$$n = \sqrt{\frac{\mu_i}{a_i^3}}.$$

Rearranging for μ_i yields

$$\mu_i = n^2 a_i^3. \tag{20}$$

Because charge products appear in the formulation of the μ_i value of each craft, Eq. (20) can be used as a second constraint on the system. This allows for the designation of an orbital period for the formation and the semi-major axes of the individual craft orbits. As mentioned, craft 1 is used to formulate this additional constraint, though this is a somewhat arbitrary selection as craft 3 would also work. Hussein et al.[18] gives the formulation for μ_1 as

$$\mu_1 = -\frac{k_c\,(m_2 + (1+\chi)m_3)^2}{m_1(m_1+m_2+m_3)^2} Q_{12} - \frac{k_c(m_2 + (1+\chi)m_3)^2}{m_1(m_1+m_2+m_3)^3(1+\chi)^2} Q_{13}. \tag{21}$$

Notice that Eq. (21) is linear with respect to the charge products. Using this as a second constraint provides a system of two linear equations to solve for three variables. Again, this will yield an infinite number of solutions based on the null space of the system. Let us define our new system of equations as

$$[X_*]\mathbf{Q} = \mathbf{b}, \tag{22}$$

where $\mathbf{Q} = \begin{bmatrix} Q_{12} & Q_{13} & Q_{23} \end{bmatrix}^T$ and $\mathbf{b} = \begin{bmatrix} 0 & n^2 a_1^3 \end{bmatrix}^T$. The importance of using craft 1 or 3 in the formulation of the second constraint is related to the rank of $[X_*]$, which is populated using Eqs. (18) and (21). In Eq. (18), the coefficient of Q_{13} would be zero if $\chi = m_1/m_3$. The formulation of μ_2 excludes the charge product Q_{13}. If craft 2 were used in the second constraint and the right χ value was used, the $[X_*]$ matrix would not be full rank, leading to a singularity in the solution due to the fact that no constraint would be placed on Q_{13}. Using craft 1 or 3 in the second constraint guarantees that $[X_*]$ will always be full rank, ensuring a solution exists. In fact, there are an infinite number of solutions for any desired configuration, governed by a one-dimensional null space. Note that using craft 1 to develop the second constraint does not limit the potential formation geometries in any way. The introduction of a second constraint, however, has eliminated the $\mathbf{Q} = \mathbf{0}$ nominal solution. In order to explore the null space set of solutions, a nominal solution is first determined by taking the pseudoinverse of $[X_*]$, so that

$$\hat{\mathbf{Q}} = [X_*]^+\mathbf{b}. \tag{23}$$

This nominal solution does not guarantee that the $Q_{12}Q_{13}Q_{23} > 0$ inequality constraint will be satisfied. To ensure compliance with this criterion, the null space must be used. The one-dimensional null space takes the form of

$$[N_*] = \begin{bmatrix} \frac{1}{\chi^2} & -\frac{(1+\chi)^2}{\chi^2} & 1 \end{bmatrix}. \tag{24}$$

Using the null space, the set of solutions for any desired configuration is

$$Q_{12} = \hat{Q}_{12} + \gamma\frac{1}{\chi^2} \tag{25a}$$

$$Q_{13} = \hat{Q}_{13} - \gamma\frac{(1+\chi)^2}{\chi^2} \tag{25b}$$

$$Q_{23} = \hat{Q}_{23} + \gamma, \tag{25c}$$

where γ is a real number scaling parameter. The inequality constraint can be formulated in terms of the null space as

$$(\hat{Q}_{12} + \frac{1}{\chi^2}\gamma)(\hat{Q}_{13} - \frac{(1+\chi)^2}{\chi^2}\gamma)(\hat{Q}_{23} + \gamma) > 0, \tag{26}$$

which is cubic in terms of the γ parameter. This cubic inequality constraint on the charge products is similar to the Q_{ij} constraint form determined by Wang in his one-dimensional three vehicle charge feedback control study.[24] The effect of varying γ can be seen in Fig. 5. It is evident that for any nominal charge solution, an infinite number of values for γ exist that will satisfy the inequality constraint. Additionally, the line will always intersect the γ-axis three times, meaning there will always be two regions of the curve that are positive, as shown in Fig. 5.

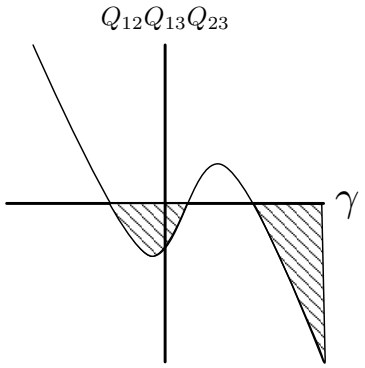

Figure 5: The inequality constraint is cubic with respect to γ, ensuring a real solution for the charges can always be found. Hatched areas represent γ values which will yield imaginary charges.

3.3. Use of L_∞ Norm for γ Selection

With an infinite number of acceptable values for γ, it is of interest to determine a method for selecting an ideal value. To do so, the γ value that corresponds with the global minimum L_∞ norm of the three craft charges is used. This has the effect of ensuring that the maximum charge on any of the craft will be as low as possible. In recognizing that the minima of the L_∞ norm correspond to points where two of the craft charges have equal values, the corresponding value for γ can be determined. Using the charge products, the magnitudes of the individual craft charges can be determined as

$$|q_1| = \sqrt{\frac{Q_{12}Q_{13}}{Q_{23}}} \tag{27a}$$

$$|q_2| = \sqrt{\frac{Q_{12}Q_{23}}{Q_{13}}} \tag{27b}$$

$$|q_3| = \sqrt{\frac{Q_{13}Q_{23}}{Q_{12}}}. \tag{27c}$$

The minima of the L_∞ norm will occur when $|q_1| = |q_2|$, $|q_1| = |q_3|$, or $|q_2| = |q_3|$. Substituting Eq. (25) into Eq. (27) provides three relationships which correspond to potential L_∞ norm minima,

$$\left(\hat{Q}_{23} + \gamma\right)^2 = \left(\hat{Q}_{13} - \gamma\frac{(1+\chi)^2}{\chi^2}\right)^2 \tag{28a}$$

$$\left(\hat{Q}_{12} + \gamma\frac{1}{\chi^2}\right)^2 = \left(\hat{Q}_{23} + \gamma\right)^2 \tag{28b}$$

$$\left(\hat{Q}_{12} + \gamma\frac{1}{\chi^2}\right)^2 = \left(\hat{Q}_{13} - \gamma\frac{(1+\chi)^2}{\chi^2}\right)^2 \tag{28c}$$

from which six corresponding γ values arise,

$$\gamma = \frac{\chi^2(\hat{Q}_{13} - \hat{Q}_{23})}{2\chi^2 + 2\chi + 1}, \frac{\chi^2(\hat{Q}_{13} + \hat{Q}_{23})}{1 + 2\chi}, \frac{\chi^2(\hat{Q}_{12} - \hat{Q}_{23})}{\chi^2 - 1}, -\frac{\chi^2(\hat{Q}_{12} + \hat{Q}_{23})}{\chi^2 + 1}, \frac{\chi^2(\hat{Q}_{13} - \hat{Q}_{12})}{\chi^2 + 2\chi + 2}, \frac{\chi(\hat{Q}_{12} + \hat{Q}_{13})}{\chi + 2}. \tag{29}$$

While the global minimum for the L_∞ norm corresponds with one of these values, it is not immediately apparent which γ it is. Furthermore, there is no guarantee that any one of these six values will produce real charge solutions.

It is entirely possible that any two of the craft charges may intersect each other in imaginary space. Once the six γ values have been found, they need to be checked against the inequality constraint in Eq. (26). Immediately, any γ values that violate this constraint can be eliminated. Another potential issue is that intersections may occur in real number space, but not at minima of the L_∞ norm. This is illustrated in Fig. 6, which shows an example of individual charge magnitudes, as well as the L_∞ norm, as a function of γ. As mentioned previously, there will be two regions on which γ will satisfy Eq. (26). These are depicted in Fig. 6. It is important that the appropriate γ value be chosen such that it corresponds to the global minimum, otherwise higher charge values than necessary will be used.

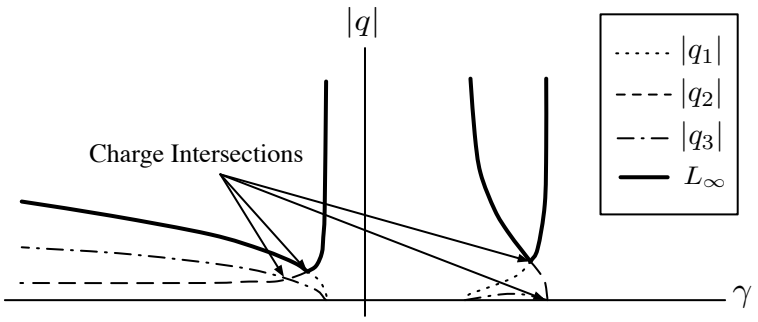

Figure 6: Example of individual craft charges and L_∞ norm as a function of γ. Charge intersections are possible at non-minima of L_∞ norm.

3.4. Finite Debye Length Case

The above analysis is extended to consider the case when the craft are in an environment with a finite Debye length. When the Debye length is low enough to affect the dynamics, the only invariant shape solutions that exist are circular orbits.[18] Thus, we may consider the determination of necessary charges for some desired circular orbit configuration of the three craft. For the first constraint Eq. (9) is used, which includes Debye length effects. The second constraint is again formulated using the effective gravitational parameter of craft one, which must be modified to include shielding effects as

$$\mu_{s1} = -\frac{k_c\,(m_2+(1+\chi)m_3)^2\left(1+\frac{r_{21}}{\lambda_D}\right)}{m_1(m_1+m_2+m_3)^2}e^{-\frac{r_{21}}{\lambda_D}}Q_{12} - \frac{k_c(m_2+(1+\chi)m_3)^2\left(1+\frac{r_{31}}{\lambda_D}\right)}{m_1(m_1+m_2+m_3)^3(1+\chi)^2}e^{-\frac{r_{31}}{\lambda_D}}Q_{13}. \tag{30}$$

Accounting for Debye length effects still yields an effective gravitational parameter that is linear in terms of the charge products. Combining this constraint with Eq. (9) results, once again, in a system of two equations for three unknowns.

The null space for the finite Debye length cases is

$$[N_D] = \begin{bmatrix} \frac{(\lambda_D+r_{32})}{(\lambda_D+r_{21})\chi^2}e^{\frac{r_{21}-r_{32}}{\lambda_D}} & -\frac{(\lambda_D+r_{32})(1+\chi)^2}{(\lambda_D+r_{31})\chi^2}e^{\frac{r_{31}-r_{32}}{\lambda_D}} & 1 \end{bmatrix} \tag{31}$$

As the Debye length becomes large relative to the separation distance, the components of the null space revert to the form seen in Eq. (24). Note that now, unlike the previous case, the null space components are dependent on the actual separation distances. When ignoring Debye shielding effects, only χ affects the null space. In an invariant shape solution χ is constant for all time, meaning the null space components will not change as the craft trajectories evolve, so long as plasma shielding effects are ignored. In Eq. (31), however, the components depend on the intercraft separation distances. This implies that if the craft were on non-circular trajectories, the null space components would be time-varying. This scenario is not possible, though, due to the fact that invariant shape solutions exist for finite Debye lengths only when the craft are on circular orbits.[18] In this case, the distances between the craft will be constant for all time, and the null space components will be constant as well.

Having identified the null space for the finite Debye length case, the solutions for the charge products may be expressed as

$$Q_{12} = \hat{Q}_{12} + \gamma \frac{(\lambda_D + r_{32})}{(\lambda_D + r_{21})\chi^2} e^{\frac{r_{21}-r_{32}}{\lambda_D}} \tag{32a}$$

$$Q_{13} = \hat{Q}_{13} - \gamma \frac{(\lambda_D + r_{32})(1+\chi)^2}{(\lambda_D + r_{31})\chi^2} e^{\frac{r_{31}-r_{32}}{\lambda_D}} \tag{32b}$$

$$Q_{23} = \hat{Q}_{23} + \gamma, \tag{32c}$$

where, again, $\hat{Q}$ is used to denote a nominal solution obtained using an inverse. As before, it is of interest to determine whether or not a real solution for the craft charges can always be found. For this analysis, return to the inequality constraint $Q_{12}Q_{13}Q_{23} > 0$. Making use of the null space, the same argument can be made for the finite Debye length case that was made before. The inequality constraint is cubic in terms of the scaling parameter γ, meaning there will always be a region on which real charges can be found.

By following the same procedure detailed above, the L_∞ optimal γ values can be found. As before, there are six potential minima of the L_∞ norm of the craft charges. Unlike before, however, they are now functions of the Debye length. The six potential optimum γ values are

$$\begin{aligned}
\gamma = &\frac{\chi^2(\hat{Q}_{12}+\hat{Q}_{13})(\lambda_D+r_{21})(\lambda_D+r_{31})e^{r_{32}/\lambda_D}}{(\lambda_D+r_{32})\left((\chi+1)^2(\lambda_D+r_{21})e^{r_{31}/\lambda_D} - e^{r_{21}/\lambda_D}(\lambda_D+r_{31})\right)}, \\
&- \frac{\chi^2(\hat{Q}_{12}-\hat{Q}_{13})(\lambda_D+r_{21})(\lambda_D+r_{31})e^{r_{32}/\lambda_D}}{(\lambda_D+r_{32})\left((\chi+1)^2(\lambda_D+r_{21})e^{r_{31}/\lambda_D} + e^{r_{21}/\lambda_D}(\lambda_D+r_{31})\right)} \\
&\frac{\chi^2(\hat{Q}_{12}-\hat{Q}_{23})(\lambda_D+r_{21})e^{r_{32}/\lambda_D}}{\chi^2(\lambda_D+r_{21})e^{r_{32}/\lambda_D} - e^{r_{21}/\lambda_D}(\lambda_D+r_{32})}, -\frac{\chi^2(\hat{Q}_{12}+\hat{Q}_{23})(\lambda_D+r_{21})e^{r_{32}/\lambda_D}}{\chi^2(\lambda_D+r_{21})e^{r_{32}/\lambda_D} + e^{r_{21}/\lambda_D}(\lambda_D+r_{32})}, \\
&\frac{(\hat{Q}_{13}+\hat{Q}_{23})\chi^2(\lambda_D+r_{31})}{(\chi+1)^2(\lambda_D+r_{32})e^{r_{21}/\lambda_D} - \chi^2(\lambda_D+r_{31})}, \frac{\chi^2(\hat{Q}_{13}-\hat{Q}_{23})(\lambda_D+r_{31})e^{r_{32}/\lambda_D}}{\chi^2(\lambda_D+r_{31})e^{r_{32}/\lambda_D} + (\chi+1)^2 e^{r_{31}/\lambda_D}(\lambda_D+r_{32})}.
\end{aligned} \tag{33}$$

Note that in the limit of $\lambda_D \to \infty$, the same γ values as in Eq. (29) are obtained.

4. Numerical Simulation

Numerical simulations of the charged relative motion differential equations in Eq. (4) are used to verify the theoretical spinning shape versus charge results developed above. Because closed orbit configurations are the focus of this research, hyperbolic and parabolic trajectories are ignored, though they are possible for a collinear invariant shape formation.[18] Instead, the design of a particular configuration is considered where the craft may take circular or elliptical trajectories about the formation center of mass. First, consider the case where the craft are desired to maintain fixed separation distances. This naturally results in circular orbits for all three craft in the formation. With circular orbits, a solution for the finite Debye length is possible. Denoting the separation distance between craft i and craft j as r_{ij}, the value of χ can quickly be determined from Eq. (8). To determine a solution for the necessary craft charges, the orbit radius of craft 1 needs to be determined. Recall that for circular orbits, the orbit radius is equal to the semimajor axis. This can be found by determining the distance between craft 1 and the formation center of mass. With χ and a_1 determined, the desired orbit mean motion, n, is all that remains to determine a set of craft charges that will yield this orbit configuration. Assuming a specific orbit period, P, is desired for the formation, the mean motion is defined as

$$n = \frac{2\pi}{P}. \tag{34}$$

As an example, consider a collinear formation where $m_1 = 100$, $m_2 = 75$, and $m_3 = 50$ kg. The craft are desired to maintain fixed separation distances of $r_{12} = 50$ and $r_{23} = 25$ m with an orbital period of 4 hrs. The resulting orbital parameters are summarized in Table 1. By defining only separation distances and an orbital period, all necessary orbital parameters can be determined. These parameters provide the necessary initial conditions which can be used

Table 1: Orbital parameters for fixed separation distances.

a_1 (m)	a_2 (m)	a_3 (m)	n (rad/sec)	χ
$33.\overline{3}$	$16.\overline{6}$	$41.\overline{6}$	$\pi/7200$	0.5

for numerical verification of the analytically predicted invariant shape motion. Because circular orbits are considered, a solution for the finite Debye-length case can be obtained. Thus, a solution for the case when λ_D=50 m will be computed and compared with the infinite Debye length case. By maintaining the same orbital geometries, only the charges on the craft will vary between the two cases. Because the Debye shielding effect weakens the electrostatic force between the craft, larger charge product magnitudes are necessary to generate the same force magnitudes

Using Eq. (23), nominal values for the charge products are determined. These values are presented in Table 2 for both the finite and infinite Debye length cases. It is evident that the nominal solutions will not satisfy the inequality constraint $Q_{12}Q_{13}Q_{23} > 0$. This is illustrated in Fig. 7(a), a plot of $Q_{12}Q_{13}Q_{23}$ as γ is varied for the infinite Debye length case. When $\gamma = 0$, which corresponds to the nominal solution, the inequality does not hold. The same is true for the finite Debye length case. As predicted, there are two regions on which γ will satisfy the inequality constraint. An acceptable value of γ must thus be selected to ensure real charges will be obtained. Using Eqs. (29) and (33), the values of γ corresponding to the minimum of the L_∞ norm are chosen. As shown in Fig. 7(b) for the infinite Debye length case, this minimum corresponds to $\gamma = -1.093 \times 10^{-11}$. The optimum γ value for the $\lambda_D = 50$ m case is -7.266×10^{-12}. Applying these values to the appropriate nullspace representations of the charge products allows for the determination of real charges, which are presented in Table 2. The shielding effects in the finite Debye length case are readily apparent, where higher charges are required to maintain the same geometry. Notice that the magnitude of q_1 is equal to that of q_2, which corresponds to

$$\gamma = \frac{\chi^2(\hat{Q}_{13} + \hat{Q}_{23})}{1 + 2\chi}.$$

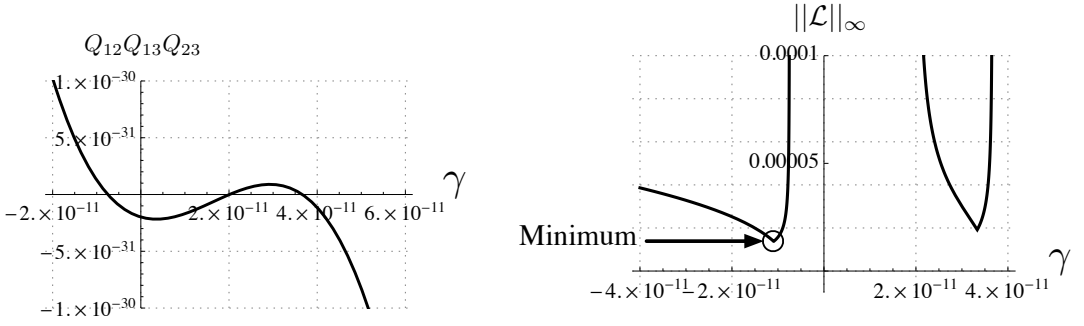

(a) Inequality Constraint

(b) $\|\mathcal{L}\|_\infty$ Norm

Figure 7: Effect of varying γ on a) inequality constraint and b) L_∞ norm for circular orbit case with infinite Debye length.

Table 2: Charge product nominal solutions and resulting charges using optimum γ for circular orbit case.

λ_D (m)	$\hat{Q}_{12}$ $(C^2) \times 10^{-10}$	$\hat{Q}_{13}$ $(C^2) \times 10^{-11}$	$\hat{Q}_{23}$ $(C^2) \times 10^{-11}$	q_1 (μC)	q_2 (μC)	q_3 (μC)	γ
∞	−1.4654	−6.7361	−2.0090	13.794	-13.794	2.249	-1.093×10^{-11}
50	−2.1488	−7.4128	−2.5259	15.837	-15.837	2.053	-7.266×10^{-12}

To verify the results, Eq. (4) is integrated numerically using appropriate initial conditions for the formation, and the charge values computed in Table 2. The trajectories are presented in Fig. 8. Note that the trajectories for the finite and infinite Debye length cases are identical, due to the fact that the same geometry is specified for both cases. As expected, the three craft take on circular orbits about the formation center of mass, with the desired separation distances. The solid black lines connecting the orbits indicate the positions of the three craft at different instances in time, demonstrating that they maintain collinearity throughout the orbit. Notice that craft 2 and 3 orbit on the opposite side of the center of mass than craft 1. This is a result of the craft masses and desired χ value of the formation.

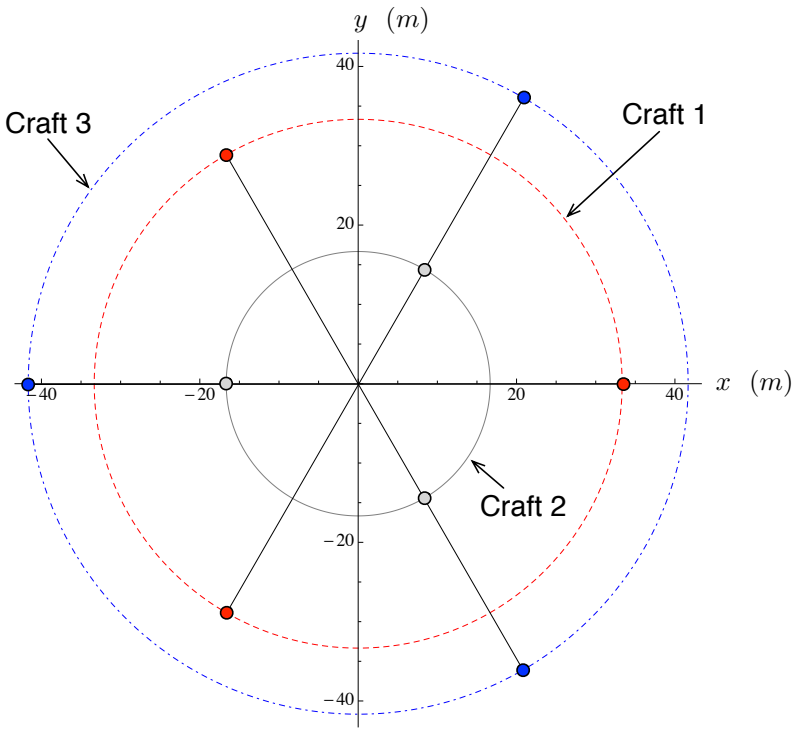

Figure 8: Circular trajectories resulting from fixed separation distances. Identical trajectories are obtained for both finite and infinite Debye lengths.

Next, the design of a formation with dynamic separation distances is considered. Assume that the craft are desired to sweep in and out over a range of separation distances, which requires elliptic orbits. Because elliptic, and not circular, orbits are specified, an infinite Debye length assumption is required. At the maximum, the craft separation distances will be $r_{12} = 50$ and $r_{23} = 25$ m, as before. This corresponds to the apoapses of the orbits. When the craft are at their closest approaches, the separation distances are desired to be $r_{12} = 40$ and $r_{23} = 20$ m. This corresponds to the orbit periapses. Note that for both of the defined separation distances, the value of χ is the same. This is a requirement for the design of any invariant shape formation configuration, because χ is constant. To determine the semi-major axes of the craft orbits, the distances from the craft to the center of mass of the formation are found at apoapsis and periapsis. Denoting these distances as r_a and r_p, respectively, the semimajor axis of craft i is determined by

$$a_i = \frac{r_{p_i} + r_{a_i}}{2}. \tag{35}$$

The orbital parameters for the corresponding craft orbits are presented in Table 3. The craft masses and orbital period are assumed to be the same as those of the circular orbit case.

The nominal solution of the charge products for the elliptic orbit case is presented in Table 4. As before, the nominal solution will not satisfy the inequality constraint $Q_{12}Q_{13}Q_{23} > 0$, as shown in Fig. 9(a). Use of the null space is required to guarantee that real charges will be obtained. Using Eq. (29), the value of γ corresponding to the

Table 3: Orbital parameters for elliptic orbits.

a_1 (m)	a_2 (m)	a_3 (m)	n (rad/sec)	χ
30	15	37.5	$\pi/7200$	0.5

minimum of the L_∞ norm is $\gamma = -7.969 \times 10^{-12}$, as illustrated in Fig. 9(b). Using this γ value, real charge solutions are obtained which are presented in Table 4

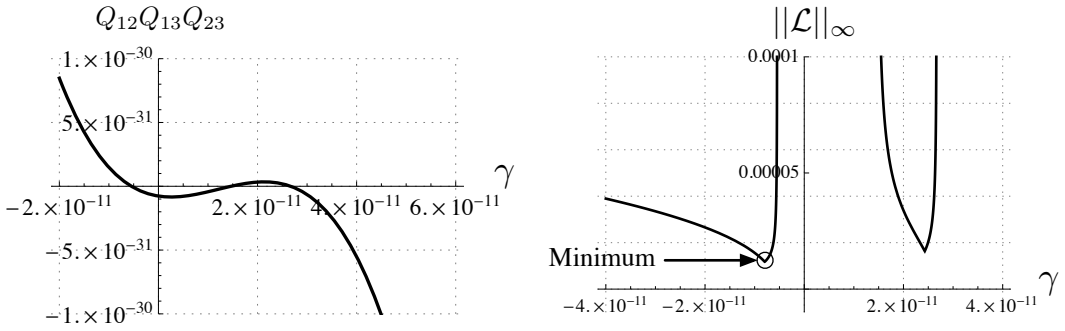

(a) Inequality Constraint

(b) $\|\mathcal{L}\|_\infty$ Norm

Figure 9: Effect of varying γ on a) inequality constraint and b) L_∞ norm for elliptic orbit case.

To simulate the trajectories for the elliptical case, initial conditions corresponding to the orbit periapses are used. To determine the required velocity the *vis-viva* equation is used, where

$$v_i = \sqrt{\frac{2\mu_i}{r_{p_i}} - \frac{\mu_i}{a_i}}. \tag{36}$$

These initial conditions are then used to obtain the trajectories from numerical integration of Eq. (4). The resulting elliptic orbits are presented in Fig. 10. Again, the solid black lines are used to connect the locations of the three craft at different instances in time, which demonstrates that the craft maintain collinearity throughout the orbit. To verify that the separation distances do in fact reach the desired levels, the separation distances are computed from the simulation results and plotted in Fig. 11. Initially, the craft are at periapsis where the desired separation distances are $r_{12} = 40$ and $r_{23} = 20$ m. From here, the craft sweep out to apoapsis, where $r_{12} = 50$ and $r_{23} = 25$ m, and back to periapsis. Thus, the desired separation distances are achieved using the charges in Table 4 and the appropriate initial conditions.

5. Conclusion

In this paper, a method is developed to solve for necessary charge levels required to maintain a desired three-craft invariant shape Coulomb formation. The formation is considered to be in deep space and no external perturbations are present. Both finite and infinite Debye length cases are considered. An equal mass configuration is analyzed, followed

Table 4: Charge product nominal solutions and resulting charges using $\gamma = -7.969 \times 10^{-12}$ for elliptic orbit case.

$\hat{Q}_{12}$ (C^2)	$\hat{Q}_{13}$ (C^2)	$\hat{Q}_{23}$ (C^2)	q_1 (μC)	q_2 (μC)	q_3 (μC)
-1.0683×10^{-10}	-4.9107×10^{-11}	-1.4646×10^{-11}	11.777	-11.777	1.920

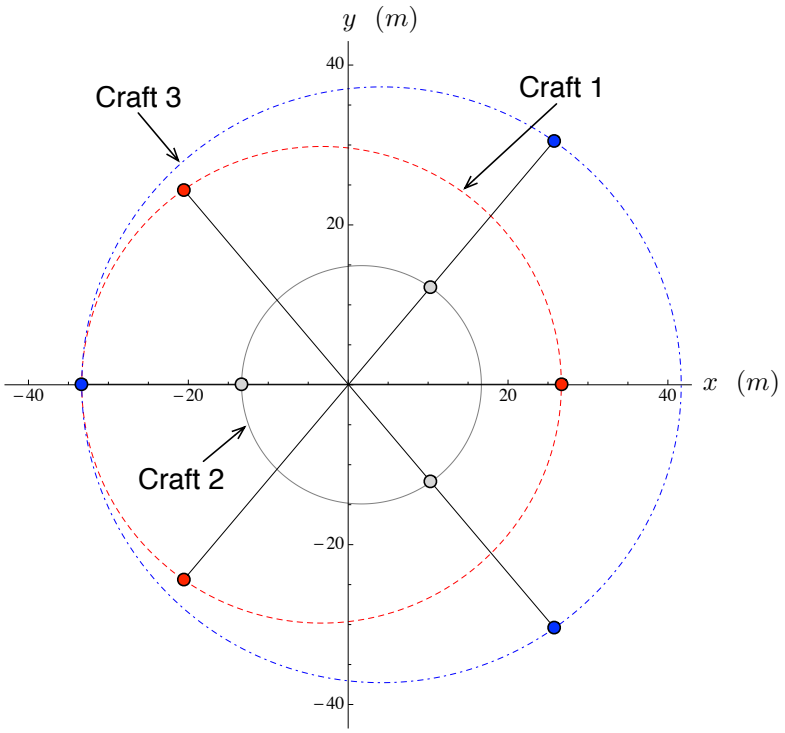

Figure 10: Elliptical trajectories of the three craft collinear formation.

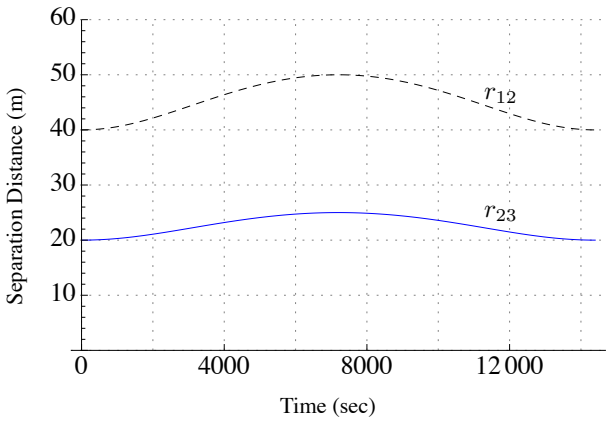

Figure 11: Separation distances over one orbital period for elliptic orbits.

by the general non-equal mass case. The underdetermined nature of the system allows for an infinite number of real charge solutions for any desired shape, whether circular or elliptic orbits are desired. Using numerical simulation, circular and elliptical invariant shapes are designed to meet required craft separation distances. Through the use of an L_∞ norm, a set of charges is chosen to minimize the maximum charge magnitude, which has important implications for power requirements on the craft. This work demonstrates that for any desired invariant shape formation geometry, real charge solutions are always possible.

References

[1] P. R. Lawson, J. A. Dooley, Technology plan for the terrestrial planet finder interferometer, Tech. Rep. JPL Publication 05-5, NASA Jet Propulsion Lab (June 2005).

[2] P. R. Lawson, O. Lay, K. J. Johnston, C. A. Beichman, Terrestrial planet finder interferometer science working group, Tech. Rep. JPL Publication 07-1, NASA Jet Propulsion Lab (March 2007).

[3] H. Schaub, G. G. Parker, L. B. King, Challenges and prospects of coulomb spacecraft formation control, Journal of the Astronautical Sciences 52 (1-2) (2004) 169–193.

[4] J. H. Cover, W. Knauer, H. A. Maurer, Lightweight reflecting structures utilizing electrostatic inflation, US Patent 3,546,706 (October 1966).

[5] L. B. King, G. G. Parker, S. Deshmukh, J.-H. Chong, Spacecraft formation-flying using inter-vehicle coulomb forces, Tech. rep., NASA/NIAC, available online at http://www.niac.usra.edu under "Funded Studies." (January 2002).

[6] L. B. King, G. G. Parker, S. Deshmukh, J.-H. Chong, Study of interspacecraft coulomb forces and implications for formation flying, AIAA Journal of Propulsion and Power 19 (3) (2003) 497–505.

[7] L. Pettazzi, D. Izzo, S. Theil, Swarm navigation and reconfiguration using electrostatic forces, in: 7th International Conference on Dynamics and Control of Systems and Structures in Space, The Old Royal Naval College, Greenwich, London, England, 2006.

[8] A. Natarjan, H. Schaub, Linear dynamics and stability analysis of a two-craft coulomb tether formation, AIAA Journal of Guidance, Control and Dynamics 29 (4) (2006) 831–839.

[9] I. I. Hussein, H. Schaub, Stability and control of relative equilibria for the three-spacecraft coulomb tether problem, Acta Astronautica 65 (5-6) (2009) 738–754.

[10] E. G. Mullen, M. S. Gussenhoven, D. A. Hardy, Scatha survey of high-voltage spacecraft charging in sunlight, Journal of the Geophysical Sciences 91 (1986) 1074–1090.

[11] H. B. Garrett, S. E. DeFrost, An analytical simulation of the geosynchronous plasma environment, Planetary Space Science 27 (1979) 1101–1109.

[12] H. B. Garrett, D. C. Schwank, S. E. DeFrost, A statistical analysis of the low energy geosynchronous plasma environment. -i electrons, Planetary Space Science 29 (1981a) 1021–1044.

[13] H. B. Garrett, D. C. Schwank, S. E. DeFrost, A statistical analysis of the low energy geosynchronous plasma environment. -i protons, Planetary Space Science 29 (1981b) 1045–1060.

[14] K. Torkar, W. Riedler, C. P. Escoubet, M. Fehringer, R. Schmidt, G. R. J. L., H. Arends, F. Rudenauer, W. Steiger, B. T. Narheim, K. Svenes, R. Torbert, A. M., A. Fazakerley, R. Goldstein, R. C. Olsen, A. Pedersen, E. Whipple, H. Zhao, Active spacecraft potential control for cluster – implementation and first results, Annales Geophysicae 19 (10/12) (2001) 1289–1302.

[15] C. P. Escoubet, M. Fehringer, M. Goldstein, The cluster mission, Annales Geophysicae 19 (10/12) (2001) 1197–1200.

[16] J. Berryman, H. Schaub, Analytical charge analysis for 2- and 3-craft coulomb formations, Journal of Guidance, Navigation and Control 30 (6).

[17] H. Schaub, C. Hall, J. Berryman, Necessary conditions for circularly-restricted static coulomb formations, Journal of the Astronautical Sciences 54 (3–4) (2006) 525–541.

[18] I. I. Hussein, H. Schaub, Invariant shape solutions of the spinning three craft coulomb tether problem, Journal of Celestial Mechanics and Dynamical Astronomy 96 (2) (2006) 137–157.

[19] J. Bittencourt, Fundamentals of Plasma Physics, Springer-Verlag New York, Inc, 2004.

[20] T. I. Gombosi, Physics of the Space Environment, Cambridge University Press, New York, NY, 1998.

[21] N. Murdoch, D. Izzo, C. Bombardelli, I. Carnelli, A. Hilgers, D. Rodgers, Electrostatic tractor for near earth object deflection, in: 59th International Astronautical Congress, 2008.

[22] J.-L. Lagrange, Essai sur le probléme des trois corps, in: Oeuvres de Lagrange, Vol. 6, Gauthiers-Villars, Paris, 1873, pp. 229–331.

[23] H. Schaub, J. L. Junkins, Analytical Mechanics of Space Systems, 2nd Edition, AIAA Education Series, Reston, VA, 2009.

[24] S. Wang, H. Schaub, 1-d constrained coulomb structure stabilization with charge saturation, in: AAS/AIAA Astrodynamics Specialist Conference, Mackinac Island, MI, 2007, Paper No. AAS 07–267.